
EXPLAINABLE LIFELONG STREAM LEARNING BASED ON “GLOCAL” PAIRWISE FUSION

Chu Kiong Loo *

Faculty of Computer Science and Information Technology
Universiti Malaya
Kuala Lumpur, Malaysia
ckloo.um@um.edu.my

Wei Shiung Liew

Faculty of Computer Science and Information Technology
Universiti Malaya
Kuala Lumpur, Malaysia
liew.wei.shiung@um.edu.my

Stefan Wermter

Knowledge Technology
Department of Informatics
Universität Hamburg
Hamburg, Germany
stefan.wermter@informatik.uni-hamburg.de

ABSTRACT

Real-time on-device continual learning applications are used on mobile phones, consumer robots, and smart appliances. Such devices have limited processing and memory storage capabilities, whereas continual learning acquires data over a long period of time. By necessity, lifelong learning algorithms have to be able to operate under such constraints while delivering good performance. This study presents the Explainable Lifelong Learning (ExLL) model, which incorporates several important traits: 1) learning to learn, in a single pass, from streaming data with scarce examples and resources; 2) a self-organizing prototype-based architecture that expands as needed and clusters streaming data into separable groups by similarity and preserves data against catastrophic forgetting; 3) an interpretable architecture to convert the clusters into explainable IF-THEN rules as well as to justify model predictions in terms of what is similar and dissimilar to the inference; and 4) inferences at the global and local level using a pairwise decision fusion process to enhance the accuracy of the inference, hence “Glocal Pairwise Fusion.” We compare ExLL against contemporary online learning algorithms for image recognition, using OpenLoris, F-SIOL-310, and Places datasets to evaluate several continual learning scenarios for video streams, low-sample learning, ability to scale, and imbalanced data streams. The algorithms are evaluated for their performance in accuracy, number of parameters, and experiment runtime requirements. ExLL outperforms all algorithms for accuracy in the majority of the tested scenarios.

Keywords Explainable AI · Interpretability · Prototype-Based Models · Lifelong Learning · Streaming Learning · Transfer Learning · Knowledge Engineering · Self-Organizing Neural Networks

1 Introduction

In most real-world applications, data arrives continuously in real-time and is often non-repeating unless it is memorized. From this phenomenon, two paradigms are coined: continuous learning and streaming learning. Continuous learning, also known as lifelong learning [1] refers to the ability to acquire knowledge continuously over a long period of time while retaining previously-learned knowledge. Streaming learning [2] on the other hand is the ability to acquire knowledge from sequential and continuously-arriving data streams. The former encompasses machine learning

*Corresponding author

techniques to adapt and reconcile old and new knowledge while minimizing loss of information and the latter prioritizes quick and efficient knowledge acquisition from high-velocity data streams.

When developing machine learning applications for use in embedded systems such as portable digital devices, robots, autonomous vehicles, and smart appliances, not only it is necessary for the applications to have both continuous and streaming learning capabilities, but also the ability to operate in resource-limited environments. Portable devices prioritize compactness which limits how much hardware can be installed on-board the device, thus limiting its processing power, memory storage, and energy storage capabilities. Example applications include portable medical devices which use continuous learning to personalize the diagnosis based on long-term monitoring of a patient’s vital signs [3]. Personalized action recognition systems adapt to individual variances in body movements [4]. On-device learning is preferable to ensure greater customization based on the consumer’s needs, as opposed to cloud-based learning where a consumer’s personalized data may be considered an insignificant detail among many other consumers’ data. There are several other benefits to continual on-device learning, such as decreased bandwidth requirements, better control over the consumer’s privacy, and less dependence on big data.

Conventional learning strategies minimize empirical risk by assuming a given dataset consists of independent and identically-distributed (iid) samples and shuffling them before training. In continuous learning however, this may sometimes cause catastrophic forgetting whereby learning new knowledge causes older learned knowledge to be forgotten [5]. While there have been many research studies to address catastrophic forgetting, not all are suitable for embedded applications.

Recent research also stresses the need for interpretability or explainability especially for machine learning algorithms used in critical applications that directly affect human well-being. The main criterion of an explainable learning model is being able to show its thought-processes step-by-step from the input to the final decision, improving human trust in the system [6] [7] and debug potentially problematic decisions [8]. The current generation of continual learning systems lacks the ability to self-diagnose their decisions. A common problem involving self-supervised or unsupervised learning systems is when the data stream consists of undetected bias or garbage data, which would negatively impact the model. By implementing explainability in continual learning models, it would be possible to debug the learning process and identify problematic data before use. As of the time of writing this paper, state-of-the-art continual learning architectures such as Streaming Linear Discriminant Analysis (SLDA) [9] did not have explainability capabilities while explainable learning architectures such as the eXplainable Deep Neural Networks (xDNN) [10] have been tested with several continuous learning scenarios but not under streaming learning conditions [11].

We argue the need for the following capabilities in streaming, explainable, continually learning architectures:

1. Learn from a continuous data stream in a single pass in environments where computational resources and data storage is highly constrained.
2. Acquire knowledge from data in any order while maintaining resilience against loss of previously learned information.
3. Learn efficiently and generalize well with minimal labeled examples.
4. Explain model decisions at the intermediate and final stages of the decision-making process.

This study investigates explainable continual and streaming learning specifically for embedded devices. The paper presents several research contributions in this field.

1. We propose a modified SLDA architecture to utilize a prototype-based architecture to address the issues of catastrophic forgetting and the stability-plasticity dilemma, the balancing between the network’s ability to retain and integrate knowledge.
2. We introduce a collective inference strategy to enhance classification accuracy by combining inferences from two levels: local inferences at the prototype level (i.e. "Among the examples in Class A, which example is the closest match to the input?") and global inferences at the class level (i.e. "Among all the classes, which is the closest match to the input?").
3. We formulate an explainable lifelong stream learning model with single-pass learning.
4. We conduct a series of benchmark tests and observe how the proposed model performed relative to other continual learning models using established datasets and continual learning scenarios.

2 Problem Definition

Integrating explainability with online continual learning applications is challenging due to a number of factors. In online continual learning, examples are only presented once and may not be repeated unless they are stored in memory.

Online continual learning models receive limited data and have a short time to learn from them. Given the scarcity of training data and learning time, it is difficult for most explainable algorithms to accurately model the concept enough to generate adequate explanations [12].

In addition, the data obtained from the continuous learning process is constantly changing. This means that the information learned by the models may also change over time and lose relevance. While deep learning models are capable of achieving high accuracy, their opaque nature makes it a challenge to generate explanations for their predictions [13] [14].

Another major challenge is implementing online continual learning algorithms on embedded devices with limited memory capacity and processing power. This restriction makes it difficult to deploy complex algorithms or algorithms that take up a lot of storage space [15] [16].

Models that provide understandable explanations typically compromise on the accuracy of the results. Balancing between explainability and accuracy is a challenge when employing explainable methods in online continual learning applications [17].

3 Related Work

3.1 Streaming Learning

In streaming learning scenarios, machine learning algorithms are required to learn from a continuous stream of non-repeating training samples in a single pass. The algorithms must also be capable of being evaluated at any point during the stream and prior training samples are not stored for retraining. In real-life applications, contextual information may not always be available. Several prototype-based classifiers such as ARTMAPs [18] were developed to learn from non-stationary data. However, the presentation order of training data significantly affects the performance of ARTMAPs. Various methods were developed to optimize ARTMAP performance [19, 20, 21] but they were computationally intensive and therefore unsuitable for real-time applications.

Streaming Linear Discriminant Analysis (SLDA) [9] extends the conventional Linear Discriminant Analysis (LDA) architecture to support incremental learning from data streams. SLDA stores a running mean for each unique class and a shared covariance matrix. During inference, SLDA classifies a given input to the most likely class using the class means and covariance matrix. The softmax methods used with conventional neural networks are analogous to the LDA’s estimated posterior distribution [22]. Deep-SLDA [23] pairs SLDA with a convolutional neural network (CNN) acting as a feature extractor for high-dimensional inputs such as images. The performance of the model surpasses that of state-of-the-art streaming learning and incremental batch learning algorithms.

3.2 Continual Embedded / On-Device Learning

Although streaming learning algorithms have been developed to reduce catastrophic forgetting, they don’t meet certain requirements for embedded applications. Disqualifying criteria include the high storage and computation requirements of batch learning techniques, and needing task labels during inference [23] [24]. Another requirement for continual embedded learning is the ability to generalize from a very small number of training samples. Algorithms with this capability are commonly known as “low-shot” continual learning algorithms [25, 26, 27, 28].

Several CNNs were made to meet the need for on-device learning, balancing accuracy of classification with speed of processing. Networks with efficient computation and reduced memory requirements include MobileNet [29], SqueezeNet [30], ShuffleNet [31] and CondenseNet [32]. Other methods to reduce memory requirements include deep network pruning [33, 34, 35, 36], quantization [37, 38, 39, 40, 41, 42, 43], and model compression or network distillation [44] [45].

A comprehensive study was performed to compare several continual learning algorithms and CNNs as feature extractors in multiple scenarios [11]. The models were tested on their robustness to scale, on imbalanced class distribution, and on temporally correlated video streams. The models were then evaluated on the basis of classification accuracy, number of parameters, and experiment runtime. We use the same experiment protocols to evaluate the performance of our proposed continual learning model against other algorithms.

3.3 Explainable Prototype-Based Learning Models

The architecture of CNNs is designed to maximize predictive accuracy through a series of convolutional steps. CNNs are considered “black box” models due to how difficult it is to explain how they arrive at a specific classification decision for a given input. CNNs are typically interpreted post hoc: the model’s decisions are obtained first before

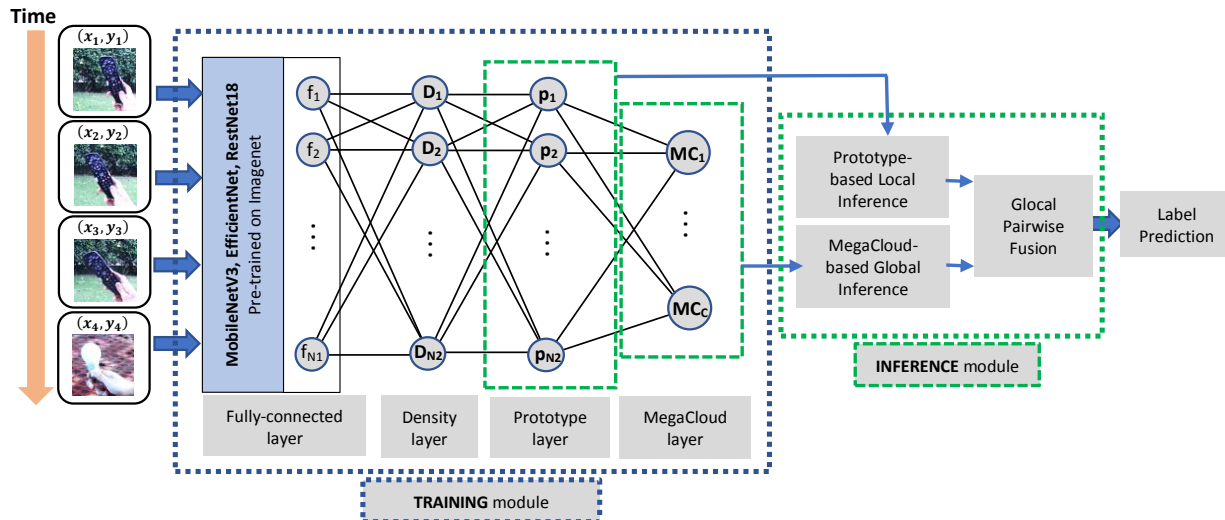


Figure 1: Explainable Lifelong Learning architecture. Training images produce feature vectors in the fully-connected layer of a pre-trained CNN. Density of the feature vectors are then computed to determine if the training images should be assigned to an existing prototype or to initialize a new prototype. All prototypes belonging to one class label are assigned to one MegaCloud. Inference is performed once at the local level, another at the global level. Local inference matches the inferred image to the most similar prototype while global inference matches the image to the most similar MegaCloud. Both inference decisions are then combined using a glocal pairwise fusion matrix to obtain the final model decision.

backtracking and generating justifications [46]. A popular explainable technique uses class activation mappings (CAMs) and gradient-weighted CAMs (Grad-CAMs) [47] [48] to highlight discriminative features on input images. Such post hoc interpretability techniques are usually approximations as opposed to in-depth explanations of the cause-and-effect relations and reasoning.

Prototype-based classifiers such as ARTMAPs [18] and self-organizing networks [49] group training samples according to their proximity in the feature space [50]. Each group or cluster of training samples can be represented by the closest centroid or prototype [51].

xDNN [10] is a prototype-based classifier with the ability to generate explanations for deep neural networks. The prototypes in the architecture are used to generate linguistic IF-THEN rules. xDNN employs empirically derived probability distribution functions based on local densities and global multivariate generative distributions [52]. The prototype-based architecture and algorithm are suitable for transfer learning and continuous learning without retraining. xDNN outperforms state-of-the-art approaches in accuracy and computational simplicity in benchmark tests [10] [53]. To summarize, xDNN is an explainable feed-forward neural network with an incremental learning algorithm adding new prototypes to reflect the dynamic data stream [54].

4 Methodology

The proposed Explainable Lifelong Learning (ExLL) model is a feed-forward neural network with an incremental learning algorithm and a self-organizing topology. Inputs to the network are typically images passed through a convolutional neural network to extract both abstract and discriminative features from the fully-connected layer. The architecture of ExLL enhances the functionality of the xDNN [10] with a few modifications for implementing a variant of SLDA [9], namely MegaCloud-based global inference and prototype-based local inference. A pairwise fusion method [55] is used to combine the global and local inferences into a “glocal” inference.

4.1 Training the Explainable Continual Learning Model

Figure 1 shows the ExLL model’s layers. CNN weights are pre-trained with image datasets such as ImageNet. Images are passed through the CNN, and the activations of the last hidden fully-connected layer in the CNN are taken as the discriminative feature vectors to be learned by the ExLL.

Similar to xDNN, the two main components of the proposed model are the Prototypes Layer and the MegaClouds Layer [10]. Input feature vectors are represented as data points in a multi-dimensional topology. Data points that are close to each other can be considered as a ‘‘data cloud’’ encompassing an area of influence between the data points. A data cloud can be represented by a composite feature vector known as a centroid or ‘‘prototype’’, calculated as the average of all points in the data cloud. A prototype is typically assigned a class label based on the labels of the majority points in the data cloud. Each prototype is independent and distinct from each other, representing the local peaks of the data distribution sharing the same class label.

Furthermore, adjacent data clouds sharing the same class label can be grouped into a larger structure known as a ‘‘MegaCloud’’. Where a prototype represents an instance-based prototype of a class label, a MegaCloud is a category-based prototype of the class label.

Training the ExLL takes place as follows:

1. An image I_i at time stamp i and belonging to class k is passed through a CNN. The subsequent feature vector \tilde{x}_i is obtained from the fully-connected layer, and then normalized:

$$x_i = \frac{\tilde{x}_i}{\|\tilde{x}_i\|} \quad (1)$$

where $\|\cdot\|$ is the vector norm.

2. The ExLL’s global meta-parameters are updated:

$$\begin{aligned} \hat{\mu}_i &= \frac{i-1}{i}\hat{\mu}_{i-1} + \frac{1}{i}x_i \\ \hat{\mu}_1 &= x_1 \end{aligned} \quad (2)$$

$$\begin{aligned} \hat{\sigma}_i &= \frac{i-1}{i}\hat{\sigma}_{i-1} + \frac{1}{i}\|x_i\|^2 \\ \hat{\sigma}_1 &= \|x_1\|^2 = 1 \end{aligned} \quad (3)$$

$$\begin{aligned} \hat{\xi}_i &= \frac{i-1}{i}\hat{\xi}_{i-1} + \frac{1}{i}(x_i - \hat{\mu}_i)(x_i - \hat{\mu}_i)^T \\ \hat{\xi}_1 &= (x_1)(x_1)^T \end{aligned} \quad (4)$$

where $\hat{\mu}$ is the global average of all training samples, $\hat{\sigma}$ is the global variance, and $\hat{\xi}$ is the inter-class global covariance matrix.

3. While the global meta-parameters represent the cross-class topology of the ExLL, local meta-parameters represent the within-class topologies for each class. If x_i has a novel class, the number of unique class labels is incremented, $k \leftarrow k + 1$, and the local meta-parameters for the new class k are initialized as follows:

$$\begin{aligned} i_k &\leftarrow 1 \\ g_k &\leftarrow 1 \\ \mu_{k,1} &\leftarrow x_i \\ \sigma_{k,1} &\leftarrow \|x_i\|^2 \\ E_{k,1,1} &= 0 \end{aligned} \quad (5)$$

Here i_k denotes the number of inputs where class k was observed during training, g_k counts the prototypes in class k , $\mu_{k,1}$ is the class mean, $\sigma_{k,1}$ is the class scalar product, and $E_{k,1,1}$ is a topological map of edge connections between within-class prototypes.

Additionally, the novel class is used to initialize the first prototype of a new MegaCloud:

$$\begin{aligned} p_{k,1} &\leftarrow x_i \\ S_{k,1} &\leftarrow 1 \\ r_{k,1} &\leftarrow r^* \\ \hat{I}_{k,1} &\leftarrow I_i \end{aligned} \quad (6)$$

where $p_{k,1}$ is the first prototype for class k , $S_{k,1}$ is the number of training samples associated with the prototype, $r_{k,1}$ is the prototype’s radius of influence initialized to a default value $r^* = \sqrt{2 - 2 \cos 30^\circ}$ [52],

and $\hat{I}_{k,1}$ keeps a record of all input images associated with this prototype, without actually storing the images themselves. The network then waits for the next input.

However, if the input presents a known class, then the prototype layer is updated in response. The local meta-parameters are updated similar to the global meta-parameters as follows:

$$\mu_{k,i_k} = \frac{i_k - 1}{i_k} \mu_{i_k-1} + \frac{1}{i_k} x_i \quad (7)$$

$$\sigma_{k,i_k} = \frac{i_k - 1}{i_k} \sigma_{i_k-1} + \frac{1}{i_k} \|x_i\|^2 \quad (8)$$

Class k 's mean μ_{k,i_k} and scalar product σ_{k,i_k} are updated online. The input x_i is then passed to the density layer.

4. **Density layer.** This layer defines the mutual proximity of the training images relative to the data space defined by the feature vectors. The density of input x_i relative to class k , $D(k, x_i)$ can be computed online [56]:

$$D(k, x_i) = \frac{1}{1 + \|x_i - \mu_{k,i_k}\|^2 + \sigma_{k,i_k} - \|\mu_{k,i_k}\|^2} \quad (9)$$

5. **Prototype layer.** When an input x_i is presented, the nearest and second-nearest within-class prototypes, b_1 and b_2 , are identified using Mahalanobis distance [57]:

$$b_1 = \underset{j=1,\dots,g_k}{\operatorname{argmin}} \frac{(x_i - p_j)^T (x_i - p_j)}{\hat{\xi}} \quad (10)$$

$$b_2 = \underset{j=1,\dots,g_k; j \neq b_1}{\operatorname{argmin}} \frac{(x_i - p_j)^T (x_i - p_j)}{\hat{\xi}} \quad (11)$$

A density condition then tests if x_i is inside the distribution of existing prototypes:

$$\text{IF } D(k, x_i) > \max_{j=1,\dots,g_k} D(k, p_j)$$

$$\text{OR } D(k, x_i) < \min_{j=1,\dots,g_k} D(k, p_j) \quad (12)$$

THEN add a new data cloud ($g_k \leftarrow g_k + 1$)

If Condition 12 is met, then the input x_i is considered outside the influence radius of the current prototypes and is sufficiently novel. x_i is then used to initialize a new data cloud:

$$\begin{aligned} g_k &\leftarrow g_k + 1 \\ \mathbf{S}_{k,g_k} &\leftarrow 1 \\ p_{k,g_k} &\leftarrow x_i \\ r_{k,g_k} &\leftarrow r_0 \\ \hat{I}_{k,g_k} &\leftarrow I_i \\ E_{k,g_k,b_1} &\leftarrow 1; E_{k,b_1,g_k} \leftarrow 1; \end{aligned} \quad (13)$$

Otherwise, if Condition 12 is not met, the parameters are updated for the closest matching prototype b_1 :

$$\begin{aligned} \mathbf{S}_{k,b_1} &\leftarrow \mathbf{S}_{k,b_1} + 1; \\ p_{k,b_1} &\leftarrow \frac{\mathbf{S}_{k,b_1} - 1}{\mathbf{S}_{k,b_1}} p_{k,b_1} + \frac{1}{\mathbf{S}_{k,b_1}} x_i; \\ r_{k,b_1} &\leftarrow \sqrt{\frac{r_{k,b_1}^2 + (1 - \|p_{k,b_1}\|^2)}{2}} \\ \hat{I}_{k,b_1} &\leftarrow \hat{I}_{k,b_1} + I_i \\ E_{k,b_1,b_2} &\leftarrow E_{k,b_1,b_2} + 1 \\ E_{k,b_2,b_1} &\leftarrow E_{k,b_2,b_1} + 1 \end{aligned} \quad (14)$$

E_k is a square matrix sized g_k for encoding the edges between local prototypes. Whenever a training sample activates the closest prototype b_1 and second-closest prototype b_2 , E_{k,b_1,b_2} and E_{k,b_2,b_1} are incremented. The

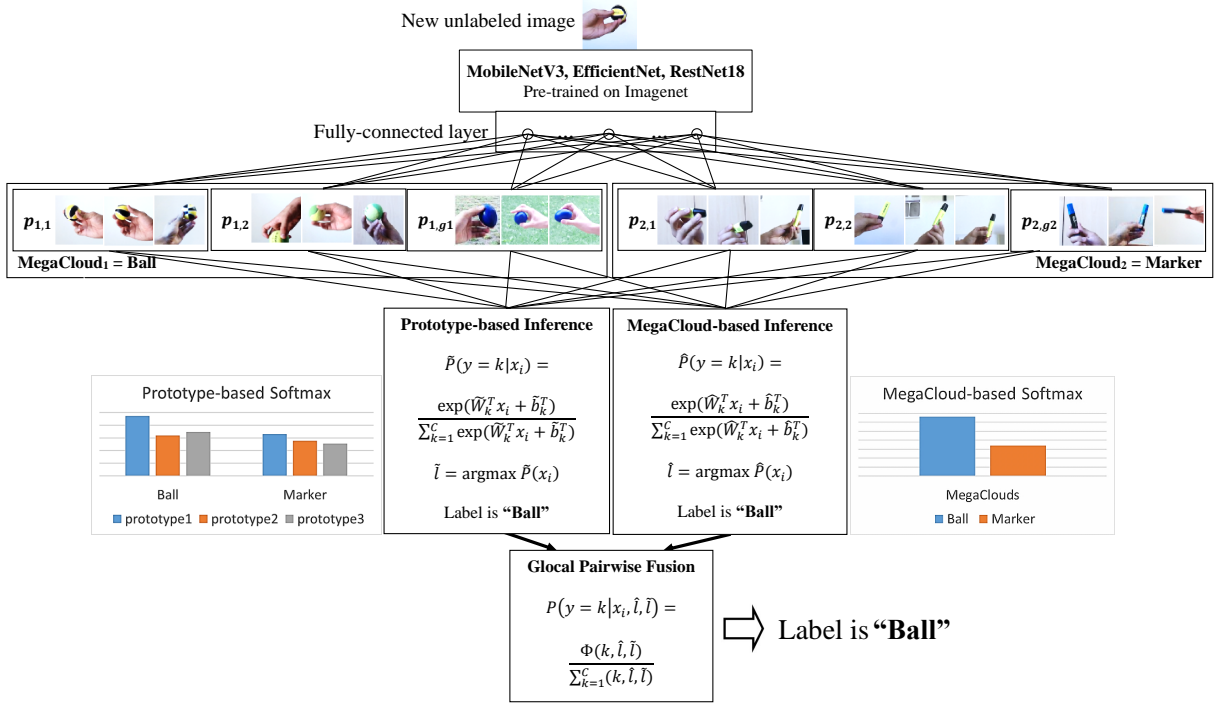


Figure 2: The process of image inference for the proposed ExLL.

map E_k can then be used for visual evaluation of the spatial relationship between prototypes or for encoding frame of reference transformations [58] with each prototype representing one frame of reference.

The prototype layer is the basis of local explainability of the ExLL model. Each prototype is an independent and distinct centroid shaped by associated training inputs. As each prototype records the associated training images in \hat{I} , a set of linguistic IF-THEN rules are formulated as:

$$R_c : \text{IF } (I \sim \hat{I}_{k,1}) \text{ OR } \dots \text{ OR } (I \sim \hat{I}_{k,g_k}) \\ \text{THEN (class is } k) \quad (15)$$

where \sim indicates similarity or fuzzy degree of membership to a prototype, $k = \{1, \dots, C\}$ is the class, and I_i denotes an input image.

6. **MegaClouds** layer. This layer is the basis of global explainability of the ExLL model. Each MegaCloud is used to facilitate explainability at the class level. Explainable rules generated from MegaClouds have the following format:

$$R_k : \text{IF } (x_i \sim \text{MC}_k) \text{ THEN (class is } k) \quad (16)$$

where MC_k is the MegaCloud for the class k .

4.2 Inferring the Explainable Continual Learning Model

Figure 2 illustrates the process where a given image is inferred. Prototype-based inference (PrInf) considers the local discriminative ability between individual prototypes while MegaCloud-based inference (McInf) globally discriminates between classes. Both types of inference have their strengths and weaknesses which adapt depending on the class distribution of the used dataset.

Pairwise fusion (PF) is used as a method for combining local and global inferences to achieve better performance than either technique alone, hence the term “glocal pairwise fusion”. A PF matrix encodes the association between PrInf and McInf during training without prior knowledge of the performance of either technique or the distribution of the dataset.

1. Shrinkage regularization is used to compute the precision matrix from the covariance matrix $\hat{\xi}$:

$$\Lambda = [(1 - \epsilon)\hat{\xi} + (\epsilon)I]^{-1} \quad (17)$$

where I is an identity matrix and $\epsilon = 1e^{-4}$ regulates shrinkage.

2. **Prototype-based inference** assembles the prototypes of a class k , $\tilde{p}_k = \{p_{1,1}, \dots, p_{k,g_k}\}$, and Λ to construct local weights \tilde{W}_k and local bias \tilde{b}_k :

$$\begin{aligned}\tilde{W}_k &= \Lambda \tilde{p}_k \\ \tilde{b}_k &= -\frac{1}{2}(\tilde{p}_k \cdot \tilde{W}_k)\end{aligned}\quad (18)$$

Subsequently, the posterior distribution \tilde{P} and label prediction \tilde{l} are formulated as follows:

$$\begin{aligned}\tilde{P}(y = k|x_i) &= \frac{\exp(\tilde{W}_k^T x_i + \tilde{b}_k^T)}{\sum_{k=1}^C \exp(\tilde{W}_k^T x_i + \tilde{b}_k^T)} \\ \tilde{l} &= \operatorname{argmax}_{k=1, \dots, C} \tilde{P}(y = k|x_i)\end{aligned}\quad (19)$$

3. **MegaCloud-based inference** assembles all class mean vectors $\hat{\mu} = \{\mu_1, \dots, \mu_C\}$, and Λ to construct global weights \hat{W} and bias \hat{b} :

$$\begin{aligned}\hat{W} &= \Lambda \hat{\mu} \\ \hat{b} &= -\frac{1}{2}(\mu \cdot \hat{W})\end{aligned}\quad (20)$$

and the subsequent posterior distribution \hat{P} and label prediction \hat{l} are formulated as follows:

$$\begin{aligned}\hat{P}(y = k|x_i) &= \frac{\exp(\hat{W}_k^T x_i + \hat{b}_k^T)}{\sum_{k=1}^C \exp(\hat{W}_k^T x_i + \hat{b}_k^T)} \\ \hat{l} &= \operatorname{argmax}_{k=1, \dots, C} \hat{P}(y = k|x_i)\end{aligned}\quad (21)$$

4. **Glocal pairwise fusion** [55] is used for combining the two inferences. During training, given an input vector’s class k_i , the local class prediction \tilde{l} , and the global class prediction \hat{l} , pairwise fusion encodes the relationship as:

$$\Phi(k_i, \hat{l}, \tilde{l}) \leftarrow \Phi(k_i, \hat{l}, \tilde{l}) + 1 \quad (22)$$

where Φ is a 3-dimensional matrix encoding the cumulative interactions between the actual label and the predicted labels from the local PrInf predictions and from the global McInf predictions. Φ is updated online as additional training inputs are presented. Other rules for updating the matrix, such as using confidence-based increments [55], can be applied instead of simplified increments.

When performing inference on an object x_i with an unknown class, global inference \hat{l} , local inference \tilde{l} , and Φ are used for estimating the glocal class probabilities $P(y = k|x_i, \hat{l}, \tilde{l})$ and glocal label prediction L :

$$\begin{aligned}P(y = k|x_i, \hat{l}, \tilde{l}) &= \frac{\Phi(k, \hat{l}, \tilde{l})}{\sum_{k=1}^C \Phi(k, \hat{l}, \tilde{l})} \\ L &= \operatorname{argmax}_{k=1, \dots, C} (P(y = k|x_i, \hat{l}, \tilde{l}))\end{aligned}\quad (23)$$

4.3 Explainability: Inference and Rule Generation

ExLL incorporates the element of explainability at the inference stage, so that label predictions can be explained in terms of ‘‘Hits’’, ‘‘Near Hits’’ and ‘‘Near Misses’’ [59]. Given an image with a known label k to be classified, Equation 23 produces the best-matching label L_1 and second-best matching label L_2 . Going back to Equations 10 and 11, the predicted class labels L_1 and L_2 each have a best-matching prototype ($b_{L_1,1}$ and $b_{L_2,1}$) as well as a second-best matching prototype ($b_{L_1,2}$ and $b_{L_2,2}$).

As explained in Equations 13 and 14, each prototype g_k is updated with a record of all associated training images: \hat{I}_{g_k} . When the winning prototype $b_{L_1,1}$ is selected for the winning label L_1 during inference, $\hat{I}_{b_{L_1,1}}$ is referenced to retrieve the images used to train the prototype. The retrieved images are then shown as a visual explanation, i.e. ‘‘Hit’’, as to why

Test Image	Hits	Near Hits	Near Misses
 “Shampoo” correctly predicted as “Shampoo”	 “Shampoo”	 “Shampoo”	 “Lotion”
 “Shampoo” Wrongly predicted as “Lotion”	 “Lotion”	 “Lotion”	 “Toothpaste”
 “Toothpaste” Wrongly predicted as “Shampoo”	 “Shampoo”	 “Shampoo”	 “Book”

Figure 3: Example of “Hits”, “Near Hits”, and “Near Misses” for the F-SIOL-310 dataset. The test image in the top row is an example of a True Positive result, the test image in the middle row is a False Negative result, and the test image in the bottom row is a False Positive result.

Rule #1	IF		OR		OR		OR ...	THEN Class is “Aqueduct”
Rule #2	IF		OR		OR		OR ...	THEN Class is “Aqueduct”
Rule #3	IF		OR		OR		OR ...	THEN Class is “Arch”
Rule #4	IF		OR		OR		OR ...	THEN Class is “Arch”

Figure 4: Explainable rules extracted from prototypes for the classes “Aqueduct” and “Arch” from Places-365. Each rule is made up of training images associated with the corresponding prototype.

the inferred image is assigned to the best-matching prototype. Where the best-matching prototype is selected based on spatial proximity, laymen can observe the retrieved images for visual comparison against the inferred image.

A similar comparison is made, “Near Hit”, by showing the training images associated with the second-best matching prototype, $\hat{I}_{b_{L1,2}}$. Lastly, “Near Miss” shows the training images associated with the winning prototype $b_{L2,1}$ for the next-best label $L_2: \hat{I}_{b_{L2,1}}$. The visual explanations provided by the “Near Hits” and “Near Misses” describe the decision boundary of the ExLL’s prediction. In edge cases where the predictions are ambiguous, the visual comparison of “Hits”, “Near Hits”, and “Near Misses” informs the user of possible alternatives.

Figure 3 demonstrates an example of a correct prediction and two wrong predictions. The top row illustrates the explanation for a True Positive prediction. An image of a shampoo bottle is correctly classified and the training images shown under “Hits” justify the selection of the best-matching prototype due to their visual similarity. The training image from the second-best matching prototype, shown under “Near Hits”, also explains why the prototype is not selected due to the visual dissimilarity to the inferred image. Lastly, “Near Misses” show why the test image is almost incorrectly classified as “Lotion” by showing the associated training images of the best prototype from the next-best class label. Given an incorrect prediction such as the False Negative result in the middle row and the False Positive result in the bottom row, the training images shown for “Hits”, “Near Hits”, and “Near Misses” explain why the ExLL made the mistake.

The records \hat{I}_{g_k} are used for visualizing explainable rules. One rule is generated from one prototype. The visualization of explainable rules reveal hidden information in each clustered prototype, as shown in Figure 4. For example, the prototype associated with Rule 1 consisted of aqueducts with clear blue skies in the background. In comparison, the training images associated with the prototype for Rule 2 do not have a visible background. Similarly, the prototype used for generating Rule 3 consists of images of arches over long hallways while the prototype for Rule 4 mainly contains images of arches with people in it. This information is not immediately visible to users since the images have been converted into feature vectors, but can be shown when the images are retrieved after training the model.

5 Experiment Setup

Given a continuous stream of images where X_t is an image at time t , a neural network classifier $F(\cdot)$ is trained incrementally using supervised online continual learning, producing a predicted label $\hat{y}_t = F(G(X_t))$. The backbone CNN $G(\cdot)$ is pre-trained on large image datasets such as the ImageNet-1k dataset [60]. Subsequently, feature vectors are obtained from the last hidden fully-connected layer in response to training images fed to $G(\cdot)$, which are then passed to $F(\cdot)$ for learning. The intermediate layers in $G(\cdot)$ are frozen after pre-training to prevent knowledge drift, i.e. the learned representations in $F(\cdot)$ are no longer up-to-date.

With this configuration, eight online continual learning strategies were studied for $F(\cdot)$ and five backbone architectures were studied for $G(\cdot)$. These studies are detailed in the following subsections.

5.1 Backbone Architectures

Three backbone CNN architectures were selected for comparison for their compact size, effectiveness, and classification accuracy when trained and tested on the ImageNet dataset.

MobileNet-v3 [61] is the successor of two previous architectures created for mobile and embedded applications [29] [62]. The CNN incorporates several strategies for efficient and accurate inference under real-time and resource-constrained scenarios. Depth-wise separable convolutions are used in conjunction with linear bottleneck layers to reduce computational cost without negatively impacting performance. Two versions are compared in this study. MobileNet-v3 Small (**MNet-S**) is more efficient but displays worse classification performance compared to MobileNet-v3 Large (**MNet-L**) which is more resource-intensive but shows better classification performance.

EfficientNet [63] utilizes neural architecture search (NAS) to automate the selection of an optimal architecture to achieve a good tradeoff between performance and model complexity. Like MobileNet-v3, EfficientNet utilizes depth-wise separable convolutions and linear bottleneck layers to reduce computational cost, making it suitable for usage in embedded and mobile applications with limited computing resources. EfficientNet refers to a family of models with varying complexity. Two models with the least complexity are compared in this study: EfficientNet-B0 (**ENet-B0**) and EfficientNet-B1 (**ENet-B1**).

ResNet [64] makes use of residual blocks allowing information to skip one or more convolutional layers and is efficient when involving very deep networks. During training, residual representations measure the differences between the actual output from each block and the desired output. Learning is performed by updating the convolutional weights to make the residual representations more accurate. ResNet includes several types of models with varying complexity. The smallest model, ResNet-18 (**RN-18**), is selected for this study as the most suitable ResNet candidate to be used in embedded systems and has been extensively tested in continual learning studies [24] [65, 66, 67, 68].

5.2 Online Continual Learning Models

We assess how well the proposed model performs when compared to seven other online continuous learning techniques for training the classifier $F(\cdot)$ using the image feature vectors extracted using $G(\cdot)$. The techniques were selected because of low memory and computation requirements and they can learn incrementally, continuously, and with a single pass.

Fine-Tune incrementally adjusts a CNN’s fully-connected layer. A stochastic gradient descent optimization strategy is used and progress is measured using cross-entropy loss of the CNN’s predictions.

Nearest Class Mean (NCM) keeps a cumulative average vector for every unique class it encounters during training. Each class mean vector is considered a prototype representing a single class. During inference, NCM compares the input feature vector to the class mean vectors using a similarity metric such as Euclidean distance. The input is assigned to the class with the most similar feature mean vector.

Streaming One-vs-Rest (SOvR) maintains a series of binary classifiers, one for each unique class it encounters during training. As each new feature vector continuously arrives in a streaming scenario, the classifier for the relevant class of the current input is updated incrementally. During inference, each classifier outputs a confidence score on whether the inferred feature vector belongs to that class. The final predicted class is selected from the classifier with the best confidence score.

Streaming Linear Discriminant Analysis (SLDA) [23] is an extension of Linear Discriminant Analysis designed to support learning from streaming data. The data distribution is modeled using class mean vectors and covariance matrices. A discriminant function is used to find a linear projection of the input data that maximizes the separation between classes. Both data distribution and discriminant function are updated incrementally as new feature vectors arrive from the data stream. During inference, SLDA uses the discriminant function to compute the probabilities of the inferred vector belonging to each of the known classes. The final predicted class is selected from the class with the best probability score.

Streaming Gaussian Naive Bayes is an extension of the Gaussian Naive Bayes algorithm designed to support learning from streaming data. The model makes use of class-conditional probability distributions to determine if a feature vector belongs to a specific class. The distribution of each feature is represented by a mean and variance. The probability distributions are updated incrementally by observing the feature values of the incoming feature vectors from the data stream. During inference, Bayes’ theorem is applied to obtain the posterior probability of each class based on the observed input feature. The predicted class is selected with the highest probability score.

Online Perceptron keeps a class vector for every unique class it encounters during training. When a feature vector is received, prediction is performed by taking the dot product of the input and the stored class vectors. The final predicted class is selected from the class with the best score. During training, no action is performed if the prediction matches the actual class. However if the prediction is a mismatch, the vector of the actual class is adjusted towards the input while the vector of the mismatched class is adjusted away from the input. This process is repeated continuously as the model receives additional feature vectors from the data stream.

Replay is a technique to reduce catastrophic forgetting by storing some of the previous training feature vectors in a memory replay buffer. During training, the model samples from incoming feature vectors equally alongside the stored feature vectors. Training examples can be selected from the buffer at random or by using specific strategies to mitigate issues such as imbalanced class representation. By incorporating past knowledge, the replay model balances the learning process to reduce catastrophic forgetting while giving equal attention to new knowledge. As training progresses, the memory buffer can be updated by replacing randomly-selected feature vectors with the current input, or by using specific strategies to retain important feature vectors. Replay can be memory intensive depending on how much storage is allocated for the memory buffer.

Explainable Lifelong Learning (ExLL) is the proposed model of this study. Three variations of the model were tested. **ExLL-P** uses Prototype-based Inference as per Equation 19 where label predictions are based on the closest prototype mean. **ExLL-M** uses MegaCloud-based Inference as per Equation 21 where label predictions are based on the closest class mean. Lastly, **ExLL-F** uses pairwise fusion to combine the label predictions from ExLL-M and ExLL-P, as per Equation 23.

5.3 Datasets

Online continual learners are evaluated using the following image classification datasets.

OpenLORIS [69] consists of videos of 40 different household items recorded from varying angles and distance, and 121 object instances across all items. Each object instance is recorded under one of the following environmental conditions: the object is surrounded by clutter; the object is illuminated by several light sources; the object is partially occluded; and the object is nearer to or further away from the camera. A total of 9 sessions are recorded for each condition and object instance. This dataset is suitable for testing a model’s ability to learn and recognize objects from dynamic and sequential image streams as well as to apply its acquired knowledge to recognize known objects under different environments.

Places-365 [70] consists of 1.8 million images of locations divided into 365 categories. The dataset is segmented into a training and validation set. This dataset is suitable for evaluating a model’s ability to learn from a large number of classes and diverse images per class.

Places-Long-Tail (Places-LT) is a subset of Places-365 with a skewed distribution of images across all classes, designed to evaluate a model’s ability to generalize from highly-imbalanced data distributions. Each of the 365 classes may consist of anywhere between 5 to thousands of images, while the validation set is identical to the validation set used by Places-365.

Few-Shot Incremental Object Learning (F-SIOL-310) [26] consists of static images of 22 household items. There are multiple instances of each item, totaling 310 object instances and 620 static images. This dataset uses two learning scenarios. The 5-shot learning scenario trains a model using only five images per class, selected at random, and tests with all other images. Likewise for the 10-shot learning scenario, only ten randomly-chosen images are used for training the model while all others are reserved as the testing set. Typically this dataset is used with multiple permutations of class orders and training images. This dataset is suitable for evaluating a model’s ability to learn from few training samples.

5.4 Experiment Protocol

One of the factors impacting the performance of an online continual learner is the order in which training data is presented. This study presents several different orderings of each dataset and we observe the effects on the learners.

Two variants of instance data orderings are used for the OpenLORIS dataset [71]. **Instance ordering** shuffles object instances before presenting all training videos to the learner for training. On the other hand, **low-shot instance ordering** presents only one training video from each object instance and category to the learner during training. Having learned from the object instances, the learners are then tested on all testing videos of known objects. The low-shot ordering method evaluates how well the learner generalizes from a limited labeled dataset to identify known objects under various environmental conditions.

For the two Places datasets, two data ordering methods are used. **Independent and identical distribution** (IID) shuffles the order of the images. **Class-IID** on the other hand organizes all the images by class; the order of the images is shuffled within each class, as well as the order of the classes. Class-IID is designed to test the learner’s ability to handle catastrophic forgetting, and is commonly used as a continual learning metric [65] [66] [68] [72]. Some learners perform poorly with Class-IID ordering if they do not have catastrophic forgetting mitigation, but are still able to perform well using IID ordering.

Lastly, F-SIOL-310 is run using Class-IID ordering for each low-shot learning scenario. The experiment is run using three permutations of class orders and the averaged results are reported over all permutations.

5.5 Performance Metric

Online continual learners are evaluated on three axes: classification accuracy, number of parameters, and experiment runtime. The performance of an online learner \mathcal{M} is computed as a modified NetScore metric [73] combining all three metrics into one score as follows:

$$\Omega(\mathcal{M}) = s \log\left(\frac{a(\mathcal{M})^\alpha}{p(\mathcal{M})^\beta c(\mathcal{M})^\gamma}\right) \quad (24)$$

where $a(\mathcal{M})$ is the learner’s testing accuracy, $p(\mathcal{M})$ is the learner’s size, $c(\mathcal{M})$ is the time taken to complete the experiment from start to finish, and α, β, γ are user-defined constants for controlling the contributions of accuracy, number of parameters, and the experiment runtime towards computing the NetScore Ω .

The NetScore parameters follow the original parameter settings as suggested by Hayes et al. [11]. $s = 20$ and $\alpha = 2$ to prioritize classification accuracy, and $\beta = \gamma = 0.25$ to moderate the large values of $p(\mathcal{M})$ and $c(\mathcal{M})$ [73]. Higher NetScores indicate better performance.

6 Results

For OpenLORIS and Places-LT, the results are reported from the average performance across three permutations for each data ordering technique. On the other hand, Places-365 is run only once for each ordering due to the long time needed to complete the experiment. Meanwhile, classifiers such as SOvR and NCM are relatively unaffected by data ordering permutations due to the usage of running class mean vectors. As for the Replay method, two buffer sizes were compared: one storing 20 training samples per class (20pc) and the other storing 2 training samples per class (2pc).

6.1 Results on OpenLORIS

Online continual learners are evaluated on OpenLORIS using two data ordering methods. **Instance ordering** trains learners on all object instances while **low-shot instance ordering** trains learners on one object instance from each object class. Performance is evaluated by combining the top-1 accuracy scores of the top-ranked choice for each learner. The scores are then averaged across all CNN architectures to compare how various orderings affect learner performance, as shown in Figure 5.

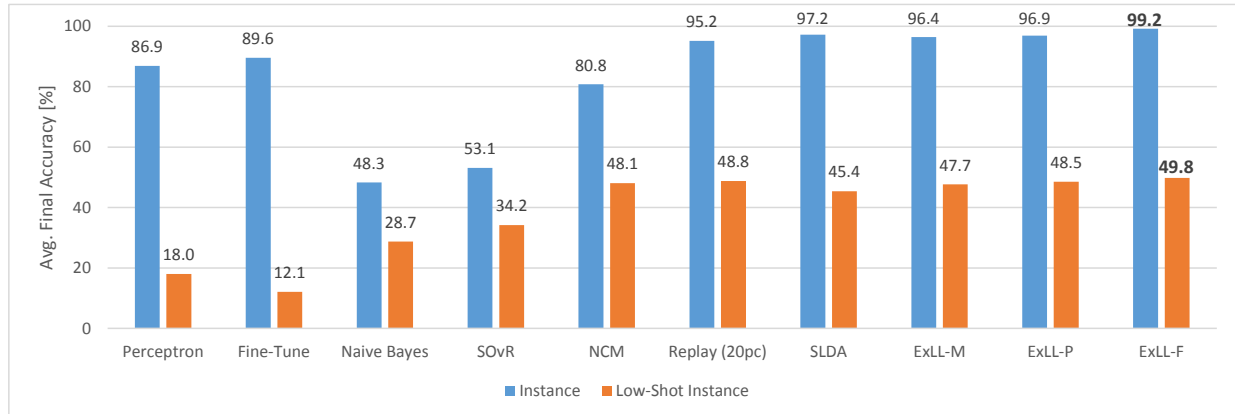


Figure 5: Accuracy results averaged across CNN architectures comparing online continual learners’ performance on OpenLORIS with **instance ordering** and **low-shot instance ordering**.

Table 1: NetScores on OpenLORIS with the **low-shot instance ordering**. **Higher** values are better. Results are highlighted as follows for the **first**, **second**, and **third** best results.

Method	MNet-S	MNet-L	ENet-B0	ENet-B1	RN-18	Mean
Perceptron	-115.9	-106.5	-91.0	-96.5	-147.8	-111.5
Fine-Tune	-149.0	-142.9	-96.3	-103.7	-187.8	-135.9
Naive Bayes	-83.7	-77.3	-75.8	-84.2	-204.5	-105.1
SOvR	-80.0	-83.9	-74.0	-78.7	-111.4	-85.6
NCM	-55.5	-64.7	-65.3	-72.5	-78.7	-67.3
Replay (20pc)	-58.9	-66.5	-66.6	-72.8	-80.5	-69.1
SLDA	-58.3	-69.1	-72.3	-79.3	-80.8	-72.0
ExLL	-75.3	-91.4	-99.5	-106.8	-108.1	-96.2

All models displayed lower accuracy when using low-shot instance ordering. Perceptron and Fine-Tune in particular showed a much bigger drop in accuracy for the low-shot instance ordering, relative to other continual learning models. The models generalized poorly when tested against images from domains not encountered during training. In comparison, Naive Bayes, SOvR, and NCM were less accurate than Perceptron and Fine-Tune for the full instance ordering, but outperformed them for the low-shot condition. The ExLL models showed the best balance between the two ordering methods, while ExLL-F outperformed all other models for both orderings.

6.1.1 NetScore Performance

In Table 1, NetScores were used for evaluating continual learning methods in terms of performance as well as memory and computational requirements. The NetScore values were obtained by evaluating all methods on the same hardware for consistency. Higher Netscore values are better.

The top three performing online continual learners are NCM, Replay 20pc, and SLDA. The NCM algorithm is the most efficient in terms of memory and computation requirements since it only stores and updates the class mean vectors. Replay 20pc needed additional computation and memory for replaying stored samples, while SLDA needed additional computation and memory for the covariance matrix. Meanwhile, ExLL was placed fifth among the eight algorithms. While ExLL is nominally similar to SLDA, ExLL required significantly more memory to store prototype mean vectors in addition to class mean vectors. In addition, ExLL stores training records to be able to recall the information for explaining inferences.

6.1.2 Backbone CNN Comparisons

Table 2 presents the best accuracy scores of online continual learning models across different CNN backbones when trained using instance ordering. The EfficientNet architectures showed the best results overall while ResNet-18 showed the worst results in eight of the ten datasets.

Table 2: Accuracy results on OpenLORIS with the **instance ordering**. Results are highlighted as follows for the **first**, **second**, and **third** best results.

Method	MNet-S	MNet-L	ENet-B0	ENet-B1	RN-18	Mean
Perceptron	0.793	0.880	0.935	0.942	0.796	0.869
Fine-Tune	0.835	0.915	0.958	0.963	0.809	0.896
Naive Bayes	0.311	0.526	0.780	0.787	0.015	0.483
SOvR	0.374	0.477	0.739	0.723	0.346	0.531
NCM	0.729	0.789	0.859	0.867	0.797	0.808
Replay (20pc)	0.921	0.956	0.977	0.978	0.929	0.952
SLDA	0.956	0.982	0.988	0.988	0.950	0.972
ExLL-M	0.944	<u>0.973</u>	<u>0.982</u>	0.982	0.940	0.964
ExLL-P	<u>0.951</u>	0.968	<u>0.982</u>	<u>0.983</u>	0.961	<u>0.969</u>
ExLL-F	0.987	0.993	0.996	0.996	0.988	0.992

Table 3: Accuracy results on OpenLORIS with the **low-shot instance ordering**. Results are highlighted as follows for the **first**, **second**, and **third** best results.

Method	MNet-S	MNet-L	ENet-B0	ENet-B1	RN-18	Mean
Perceptron	0.098	0.167	0.272	0.283	0.082	0.180
Fine-Tune	0.043	0.066	0.238	0.232	0.030	0.121
Naive Bayes	0.232	0.366	0.421	0.399	0.021	0.287
SOvR	0.259	0.323	0.449	0.459	0.224	0.342
NCM	0.442	0.474	0.516	0.514	<u>0.463</u>	0.481
Replay (20pc)	0.453	0.480	<u>0.529</u>	<u>0.532</u>	0.446	0.488
SLDA	0.445	0.454	0.472	0.460	0.442	0.454
ExLL-M	<u>0.463</u>	<u>0.493</u>	0.504	0.487	0.440	0.477
ExLL-P	0.470	0.501	0.500	0.482	0.475	0.485
ExLL-F	0.481	0.511	<u>0.511</u>	<u>0.495</u>	0.492	0.498

Table 3 presents the performance of the models across different CNN architectures for low-shot instance ordering. Compared to the previous table, classification accuracy was significantly lower due to fewer training samples. The EfficientNet backbone CNNs again outperformed the other backbone CNNs.

6.2 Results on Places-365 and Places-LT

In this section, online continual learners were compared in terms of performance, regardless of which CNN architecture was used. Tables 4 and 5 show the average top-1 accuracy for Places-365 and Places-LT, respectively, for all online continual learners across all CNNs. In almost every case, SLDA outperformed ExLL-M and ExLL-P.

However, when pairwise fusion was used for combining the results from the two ExLL methods, ExLL-F was able to outperform SLDA, ExLL-M, and ExLL-P by a significant margin. This suggests that the local and global inferences in ExLL-F contain complementary information and were able to address each other’s weaknesses when pairwise fusion is used.

Perceptron and Fine-Tune show a significant drop in accuracy in Class-IID compared to IID, due to catastrophic forgetting. When training using Class-IID, known classes are not revisited and are thus negatively impacted when new classes are introduced. Other online continual learning models, including ExLL, are not as affected by catastrophic forgetting.

Both Places datasets use the same set of images for testing but with different training sets. While Places-365 tests generalization for 365 location-based classes with 1.8 million images, Places-LT tests how well models perform with severe imbalance, with classes consisting of anywhere between 5 to 4,980 training images. Therefore, comparing the performance of the models for the two datasets is one way to observe their robustness against dataset imbalance. Of the three ExLL methods, MegaCloud-based inference was the least affected by dataset imbalance while prototype-based inference and pairwise fusion showed a 7.4% and 12.1% loss in performance respectively when trained with Places-LT. ExLL-F in particular showed worse performance compared to either ExLL-M and ExLL-P, demonstrating a significant vulnerability to imbalance.

A visualization of the topology of prototypes is provided as a supplementary material (Figure 7).

Table 4: Accuracy results on Places-365 for two data ordering methods **iid** and **class-iid**. Results are highlighted as follows for the **first**, **second**, and **third** best results.

Method	IID					Mean
	MNet-S	MNet-L	ENet-B0	ENet-B1	RN-18	
Perceptron	0.303	0.344	0.352	0.340	0.294	0.326
Fine-Tune	0.214	0.252	0.293	0.280	0.217	0.251
Naive Bayes	0.028	0.093	0.250	0.249	0.003	0.124
NCM	0.285	0.332	0.361	0.356	0.322	0.331
Replay (20pc)	0.289	0.323	0.354	0.348	0.261	0.315
SLDA	0.362	0.397	0.412	0.405	0.362	0.387
ExLL-M	0.375	0.347	<u>0.392</u>	0.336	0.312	0.352
ExLL-P	0.354	<u>0.380</u>	0.381	0.370	0.343	0.365
ExLL-F	0.444	0.478	0.488	0.476	0.440	0.465

Method	Class-IID					Mean
	MNet-S	MNet-L	ENet-B0	ENet-B1	RN-18	
Perceptron	0.004	0.003	0.012	0.013	0.005	0.007
Fine-Tune	0.003	0.003	0.006	0.006	0.003	0.004
Naive Bayes	0.028	0.093	0.250	0.249	0.003	0.124
NCM	0.265	0.309	0.336	0.329	0.300	0.307
Replay (20pc)	0.251	0.279	0.297	0.295	0.235	0.271
SLDA	0.362	0.397	0.412	0.405	0.362	0.387
ExLL-M	0.347	0.362	<u>0.381</u>	0.367	0.349	0.361
ExLL-P	<u>0.352</u>	<u>0.378</u>	<u>0.381</u>	<u>0.373</u>	0.343	<u>0.365</u>
ExLL-F	0.444	0.473	0.486	0.479	0.439	0.464

Table 5: Accuracy results on Places-LT for two data ordering methods **iid** and **class-iid**. Accuracy scores are averaged over three runs with different data permutations. Results are highlighted as follows for the **first**, **second**, and **third** best results.

Method	IID					Mean
	MNet-S	MNet-L	ENet-B0	ENet-B1	RN-18	
Perceptron	0.152	0.185	0.213	0.206	0.149	0.181
Fine-Tune	0.136	0.163	0.197	0.191	0.141	0.165
Naive Bayes	0.015	0.050	0.199	0.213	0.100	0.115
SOvR	0.089	0.149	0.262	0.245	0.146	0.178
NCM	0.265	0.309	0.336	<u>0.329</u>	<u>0.300</u>	0.306
Replay (20pc)	0.239	0.267	0.290	0.282	0.223	0.260
SLDA	0.290	<u>0.318</u>	<u>0.338</u>	0.328	<u>0.300</u>	<u>0.315</u>
ExLL-M	0.356	0.392	0.407	0.400	0.360	0.383
ExLL-P	0.265	0.297	0.315	0.305	0.277	0.292
ExLL-F	0.324	0.349	0.362	0.351	0.331	0.343

Method	Class-IID					Mean
	MNet-S	MNet-L	ENet-B0	ENet-B1	RN-18	
Perceptron	0.017	0.028	0.071	0.073	0.015	0.041
Fine-Tune	0.015	0.021	0.071	0.075	0.004	0.037
Naive Bayes	0.015	0.050	0.199	0.213	0.001	0.096
SOvR	0.089	0.149	0.262	0.245	0.146	0.178
NCM	0.265	0.309	0.336	<u>0.329</u>	<u>0.300</u>	0.308
Replay (20pc)	0.241	0.268	0.306	0.295	0.193	0.261
SLDA	0.290	<u>0.319</u>	0.338	0.328	0.300	0.315
ExLL-M	0.311	0.331	0.338	0.331	0.345	0.331
ExLL-P	0.265	0.300	0.314	0.303	0.273	0.291
ExLL-F	0.325	0.351	0.359	0.350	0.330	0.343

Table 6: Accuracy results on F-SIOL-310 using **class-iid data ordering** for **5-shot** learning and **10-shot** learning scenarios. Accuracy scores are averaged over three runs with different data permutations. Results are highlighted as follows for the **first**, **second**, and **third** best results.

Method	5-Shot					
	MNet-S	MNet-L	ENet-B0	ENet-B1	RN-18	Mean
Perceptron	0.181	0.177	0.406	0.454	0.049	0.253
Fine-Tune	0.183	0.205	0.416	0.460	0.090	0.270
Naive Bayes	0.344	0.554	0.816	0.828	0.035	0.515
SOvR	0.592	0.666	0.679	0.693	0.428	0.611
CBCL	<u>0.853</u>	<u>0.878</u>	<u>0.886</u>	0.838	0.848	0.860
NCM	<u>0.853</u>	0.871	<u>0.886</u>	0.885	0.885	<u>0.876</u>
Replay (20pc)	0.541	0.632	0.594	0.612	0.624	0.600
SLDA	0.880	0.899	0.912	0.903	<u>0.854</u>	0.889
ExLL-M	0.842	0.873	0.863	0.847	0.851	0.855
ExLL-P	0.827	0.832	0.799	0.755	0.803	0.803
ExLL-F	0.889	0.905	0.887	<u>0.854</u>	0.885	0.884

Method	10-Shot					
	MNet-S	MNet-L	ENet-B0	ENet-B1	RN-18	Mean
Perceptron	0.158	0.223	0.354	0.458	0.051	0.248
Fine-Tune	0.127	0.199	0.389	0.453	0.090	0.251
Naive Bayes	0.320	0.537	0.806	0.854	0.015	0.506
SOvR	0.561	0.702	0.650	0.752	0.504	0.633
CBCL	0.883	0.906	0.888	0.892	0.869	0.887
NCM	0.883	0.906	0.893	0.913	0.896	0.898
Replay (20pc)	0.625	0.694	0.714	0.722	0.731	0.697
SLDA	0.924	0.948	0.938	0.936	0.910	<u>0.931</u>
ExLL-M	<u>0.926</u>	<u>0.942</u>	0.938	<u>0.928</u>	0.948	0.936
ExLL-P	0.927	0.934	0.897	0.879	0.930	0.913
ExLL-F	0.961	0.966	0.952	0.943	<u>0.968</u>	0.958

6.3 Results on F-SIOL-310

F-SIOL-310 was selected to observe how the online continual learning methods perform in low-shot continuous learning applications. Table 6 presents the performance for all continual learning methods, backbone CNNs, and learning scenarios. For the 5-shot scenario, ExLL-F is slightly outperformed by SLDA (0.884 vs. 0.889 respectively). On the other hand, for the 10-shot scenario, ExLL-F significantly outperformed the next-best methods, ExLL-M and SLDA (0.958 vs. 0.936 and 0.931 respectively).

A visualization of the topology of prototypes is provided as a supplementary material (Figure 8).

6.4 Overall Results

Spider plots were generated to visualize the performance metrics of online continual learners in terms of several factors: (**NetScore**), an index representing the learner’s accuracy and memory and runtime requirements; (**Video**), the learner’s ability to learn from sequential images or videos, evaluated based on its performance for the instance-ordered OpenLORIS dataset; (**Low-Shot**), the learner’s ability to learn from a very small set of training inputs, evaluated using low-shot instance-ordered OpenLORIS; (**Scale**), its scalability to large-scale data, evaluated from Places-365; and (**Imbal.**), the learner’s performance on imbalanced datasets, evaluated using Places-LT. To construct the plots, the performance metrics of learners were averaged for all backbone architectures and then normalized by assigning 0 to the worst score and 1 to the best score.

Figure 6 illustrates the generated spider plots. The online continual learner’s name is presented at the top of each plot along with the averaged score for all five metrics. ExLL-F (0.91) showed the best overall performance. Replay 20pc (0.88) and SLDA (0.88) outperformed the second-best ExLL model, ExLL-P (0.84). The worst-performing ExLL model, ExLL-M (0.78) is also outperformed by NCM (0.81).

The ExLL models performed poorly due to having low NetScores despite having better scores in the other four metrics. While sharing some similarities with SLDA, ExLL is less efficient with respect to computation and memory

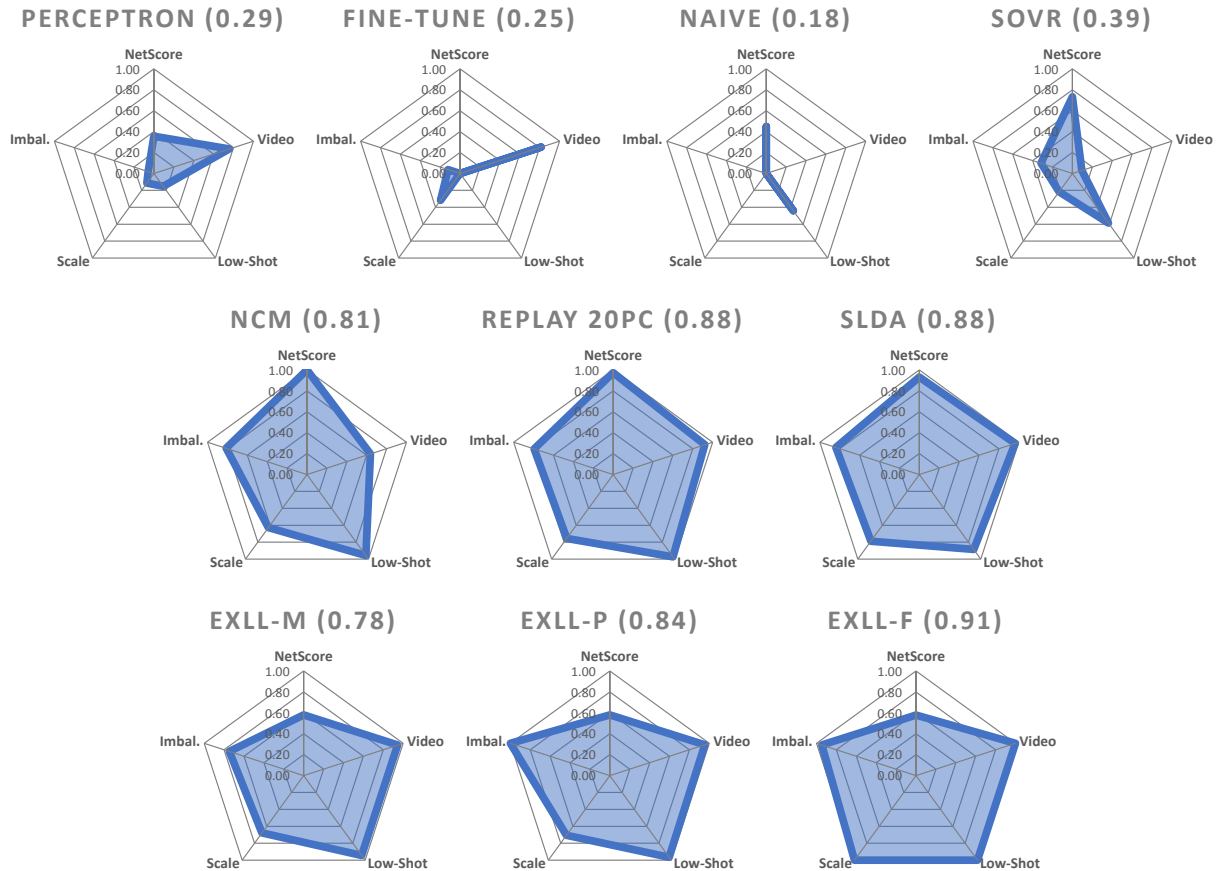


Figure 6: The normalized performance metrics of online continual learners for accuracy and memory and computation requirements (**NetScore**); learning from temporally correlated videos (**Video**); generalizing from few data samples (**Low-Shot**); scalability (**Scale**); and learning from imbalanced data distributions (**Imbal.**). The learner’s average performance across all metrics is shown at the top of each plot. **Higher** values are better.

requirements. In addition to class vector means, ExLL models store prototype vector means as well as records of training samples to facilitate post hoc explainability during inference.

7 Conclusion

We propose an explainable neural network architecture suitable for online and continual learning applications on embedded devices. The Explainable Lifelong Learning (ExLL) model is a prototype-based classifier inspired by SLDA and is robust against catastrophic forgetting and mitigates the stability-plasticity dilemma. ExLL was designed to facilitate single-pass learning from a continuous data stream. The design of the architecture also makes it easy to generate IF-THEN rules and justify the classifier decisions with highly interpretable explanations. A collective inference strategy was implemented to combine the global MegaCloud inference with the local prototype-based inference using glocal pairwise decision fusion to enhance predictive accuracy.

The classifier’s performance was benchmarked against state-of-the-art online learning models using several different CNN backbones, object recognition datasets, and evaluation metrics. In terms of video classification accuracy, low-shot learning, scalability, and imbalanced data learning, ExLL outperformed other online learning models in nearly every scenario. However, in terms of metrics to quantify the model’s storage and computational requirements, ExLL did not rank as high as Replay 20pc, SLDA, and NCM. One factor is due to these methods maintaining only one class mean per class while ExLL maintains a small topology of centroids per class as well as additional memory storage to facilitate explainability. Overall, ExLL showed state-of-the-art classification accuracy in continual learning scenarios. As for suitability for embedded applications, ExLL outperformed Perceptron, Fine-Tune, and Naive Bayes, but was ranked

below SOvR, NCM, Replay, and SLDA. This is one of the trade-offs between number of parameters and experiment runtime requirements, and the need for a prototype-based architecture for explainability.

There are several strategies that can be considered to improve ExLL’s efficiency. Pruning strategies may help identify low-utility prototypes that can be pruned without significant catastrophic forgetting, thus reducing the number of parameters requirement of the model [74, 75, 76]. Other explainability techniques can be applied to enhance interpretability, including the use of gradient class activation maps to visualize discriminative image features [47] [77]. Combined with selective feature weighing to ignore redundant features [78], this may help reduce the dimensionality and computation required by the model.

In conclusion, our research has shown that the proposed ExLL model achieved a very good performance when tested under diverse continual learning scenarios, even when compared against state-of-the-art continual learning models. Introducing the ability to explain and justify the model predictions is a necessary and important contribution for all online continual learning algorithms and that we have shown the merits of doing so.

Acknowledgments

The authors acknowledge the support from the German Research Foundation (Deutsche Forschungsgemeinschaft/DFG) under project CML (TRR 169), the TRAnsparent, InterpretabLe Robots (TRAIL) EU project, and from the BMWK under project VeriKAS.

References

- [1] Sebastian Thrun and Tom M Mitchell. Lifelong robot learning. *Robotics and Autonomous Systems*, 15(1-2):25–46, 1995.
- [2] Pedro Domingos and Geoff Hulten. Mining high-speed data streams. In *Proceedings of the Sixth ACM SIGKDD International Conference on Knowledge Discovery and Data Mining*, pages 71–80, 2000.
- [3] David Castiñeira, Katherine R Schlosser, Alon Geva, Amir R Rahmani, Gaston Fiore, Brian K Walsh, Craig D Smallwood, John H Arnold, and Mauricio Santillana. Adding continuous vital sign information to static clinical data improves the prediction of length of stay after intubation: A data-driven machine learning approach. *Respiratory Care*, 65(9):1367–1377, 2020.
- [4] German I Parisi, Sven Magg, and Stefan Wermter. Human motion assessment in real time using recurrent self-organization. In *2016 25th IEEE International Symposium on Robot and Human Interactive Communication (RO-MAN)*, pages 71–76. IEEE, 2016.
- [5] German I Parisi, Ronald Kemker, Jose L Part, Christopher Kanan, and Stefan Wermter. Continual lifelong learning with neural networks: A review. *Neural Networks*, 113:54–71, 2019.
- [6] Tatsuya Nomura and Kayoko Kawakami. Relationships between robot’s self-disclosures and human’s anxiety toward robots. In *2011 IEEE/WIC/ACM International Conferences on Web Intelligence and Intelligent Agent Technology*, volume 3, pages 66–69. IEEE, 2011.
- [7] Or Biran and Courtenay Cotton. Explanation and justification in machine learning: A survey. In *IJCAI-17 Workshop on Explainable AI (XAI)*, volume 8, pages 8–13, 2017.
- [8] Todd Kulesza, Margaret Burnett, Weng-Keen Wong, and Simone Stumpf. Principles of explanatory debugging to personalize interactive machine learning. In *Proceedings of the 20th International Conference on Intelligent User Interfaces*, pages 126–137, 2015.
- [9] Shaoning Pang, Seiichi Ozawa, and Nikola Kasabov. Incremental linear discriminant analysis for classification of data streams. *IEEE Transactions on Systems, Man, and Cybernetics*, 35(5):905–914, 2005.
- [10] Plamen Angelov and Eduardo Soares. Towards explainable deep neural networks (xDNN). *Neural Networks*, 130:185–194, 2020.
- [11] Tyler L Hayes and Christopher Kanan. Online continual learning for embedded devices. In *Proceedings of The 1st Conference on Lifelong Learning Agents*, volume 199, pages 744–766, 2022.
- [12] Oriol Vinyals, Charles Blundell, Timothy Lillicrap, Daan Wierstra, and Koray Kavukcuoglu. Matching networks for one shot learning. *Advances in Neural Information Processing Systems*, 29, 2016.
- [13] Arun Rai. Explainable AI: From black box to glass box. *Journal of the Academy of Marketing Science*, 48:137–141, 2020.

- [14] Marco Tulio Ribeiro, Sameer Singh, and Carlos Guestrin. ‘Why should I trust you?’ Explaining the predictions of any classifier. In *Proceedings of the 22nd ACM SIGKDD International Conference on Knowledge Discovery and Data Mining*, pages 1135–1144, 2016.
- [15] Nicholas D Lane, Sourav Bhattacharya, Akhil Mathur, Petko Georgiev, Claudio Forlivesi, and Fahim Kawsar. Squeezing deep learning into mobile and embedded devices. *IEEE Pervasive Computing*, 16(3):82–88, 2017.
- [16] Helena Holmström Olsson. Challenges and strategies for undertaking continuous experimentation to embedded systems: Industry and research perspectives. *Agile Processes in Software Engineering and Extreme Programming*, pages 277–292, 2018.
- [17] Gintare Karolina Dziugaite, Shai Ben-David, and Daniel M Roy. Enforcing interpretability and its statistical impacts: Trade-offs between accuracy and interpretability. *arXiv preprint arXiv:2010.13764*, 2020.
- [18] Gail A Carpenter, Stephen Grossberg, and John H Reynolds. ARTMAP: Supervised real-time learning and classification of nonstationary data by a self-organizing neural network. *Neural Networks*, 4(5):565–588, 1991.
- [19] Ramaswamy Palaniappan and Chikkanan Eswaran. Using genetic algorithm to select the presentation order of training patterns that improves simplified fuzzy ARTMAP classification performance. *Applied Soft Computing*, 9(1):100–106, 2009.
- [20] Masoud Yaghini and Mohammad Ali Shadmani. GOFAM: A hybrid neural network classifier combining fuzzy ARTMAP and genetic algorithm. *Artificial Intelligence Review*, 39:183–193, 2013.
- [21] Wei Shiung Liew, Manjeevan Seera, Chu Kiong Loo, and Einly Lim. Affect classification using genetic-optimized ensembles of fuzzy ARTMAPs. *Applied Soft Computing*, 27:53–63, 2015.
- [22] Kimin Lee, Kibok Lee, Honglak Lee, and Jinwoo Shin. A simple unified framework for detecting out-of-distribution samples and adversarial attacks. *Advances in Neural Information Processing Systems*, 31, 2018.
- [23] Tyler L Hayes and Christopher Kanan. Lifelong machine learning with deep streaming linear discriminant analysis. In *Proceedings of the IEEE/CVF Conference on Computer Vision and Pattern Recognition Workshops*, pages 220–221, 2020.
- [24] Tyler L Hayes, Kushal Kafle, Robik Shrestha, Manoj Acharya, and Christopher Kanan. Remind your neural network to prevent catastrophic forgetting. In *Computer Vision: 16th European Conference, ECCV 2020*, pages 466–483. Springer, 2020.
- [25] Ali Ayub and Alan R Wagner. Cognitively-inspired model for incremental learning using a few examples. In *Proceedings of the IEEE/CVF Conference on Computer Vision and Pattern Recognition Workshops*, pages 222–223, 2020.
- [26] Ali Ayub and Alan R Wagner. F-SIOL-310: A robotic dataset and benchmark for few-shot incremental object learning. In *2021 IEEE International Conference on Robotics and Automation (ICRA)*, pages 13496–13502. IEEE, 2021.
- [27] Xiaoyu Tao, Xiaopeng Hong, Xinyuan Chang, Songlin Dong, Xing Wei, and Yihong Gong. Few-shot class-incremental learning. In *Proceedings of the IEEE/CVF Conference on Computer Vision and Pattern Recognition*, pages 12183–12192, 2020.
- [28] Xiaoyu Tao, Xinyuan Chang, Xiaopeng Hong, Xing Wei, and Yihong Gong. Topology-preserving class-incremental learning. In *Computer Vision: 16th European Conference, ECCV 2020*, pages 254–270. Springer, 2020.
- [29] Andrew G Howard, Menglong Zhu, Bo Chen, Dmitry Kalenichenko, Weijun Wang, Tobias Weyand, Marco Andreetto, and Hartwig Adam. MobileNets: Efficient convolutional neural networks for mobile vision applications. *arXiv preprint arXiv:1704.04861*, 2017.
- [30] Forrest N Iandola, Song Han, Matthew W Moskewicz, Khalid Ashraf, William J Dally, and Kurt Keutzer. SqueezeNet: AlexNet-level accuracy with 50x fewer parameters and < 0.5 MB model size. *arXiv preprint arXiv:1602.07360*, 2016.
- [31] Xiangyu Zhang, Xinyu Zhou, Mengxiao Lin, and Jian Sun. ShuffleNet: An extremely efficient convolutional neural network for mobile devices. In *Proceedings of the IEEE Conference on Computer Vision and Pattern Recognition*, pages 6848–6856, 2018.
- [32] Gao Huang, Shichen Liu, Laurens Van der Maaten, and Kilian Q Weinberger. CondenseNet: An efficient DenseNet using learned group convolutions. In *Proceedings of the IEEE Conference on Computer Vision and Pattern Recognition*, pages 2752–2761, 2018.
- [33] Jose M Alvarez and Mathieu Salzmann. Learning the number of neurons in deep networks. *Advances in Neural Information Processing Systems*, 29, 2016.

- [34] Hengyuan Hu, Rui Peng, Yu-Wing Tai, and Chi-Keung Tang. Network trimming: A data-driven neuron pruning approach towards efficient deep architectures. *arXiv preprint arXiv:1607.03250*, 2016.
- [35] Hao Li, Asim Kadav, Igor Durdanovic, Hanan Samet, and Hans Peter Graf. Pruning filters for efficient ConvNets. In *International Conference on Learning Representations*, pages 1–13, 2017.
- [36] Christos Louizos, Max Welling, and Diederik P Kingma. Learning sparse neural networks through L_0 regularization. In *International Conference on Learning Representations*, pages 1–13, 2018.
- [37] Matthieu Courbariaux, Itay Hubara, Daniel Soudry, Ran El-Yaniv, and Yoshua Bengio. Binarized neural networks. In *Advances in Neural Information Processing Systems*, volume 29, pages 4114–4122, 2016.
- [38] Minje Kim and Paris Smaragdakis. Bitwise neural networks. *arXiv preprint arXiv:1601.06071*, 2016.
- [39] Jiaxiang Wu, Cong Leng, Yuhang Wang, Qinghao Hu, and Jian Cheng. Quantized convolutional neural networks for mobile devices. In *Proceedings of the IEEE Conference on Computer Vision and Pattern Recognition*, pages 4820–4828, 2016.
- [40] Shuchang Zhou, Yuxin Wu, Zekun Ni, Xinyu Zhou, He Wen, and Yuheng Zou. DoReFa-Net: Training low bitwidth convolutional neural networks with low bitwidth gradients. *arXiv preprint arXiv:1606.06160*, 2016.
- [41] Aojun Zhou, Anbang Yao, Yiwen Guo, Lin Xu, and Yurong Chen. Incremental network quantization: Towards lossless CNNs with low-precision weights. In *International Conference on Learning Representations*, pages 1–14, 2017.
- [42] Benoit Jacob, Skirmantas Kligys, Bo Chen, Menglong Zhu, Matthew Tang, Andrew Howard, Hartwig Adam, and Dmitry Kalenichenko. Quantization and training of neural networks for efficient integer-arithmetic-only inference. In *Proceedings of the IEEE Conference on Computer Vision and Pattern Recognition*, pages 2704–2713, 2018.
- [43] Raghuraman Krishnamoorthi. Quantizing deep convolutional networks for efficient inference: A whitepaper. *arXiv preprint arXiv:1806.08342*, 2018.
- [44] Cristian Buciluă, Rich Caruana, and Alexandru Niculescu-Mizil. Model compression. In *Proceedings of the 12th ACM SIGKDD International Conference on Knowledge Discovery and Data Mining*, pages 535–541, 2006.
- [45] Geoffrey Hinton, Oriol Vinyals, and Jeff Dean. Distilling the knowledge in a neural network. *arXiv preprint arXiv:1503.02531*, 2015.
- [46] Oscar Li, Hao Liu, Chaofan Chen, and Cynthia Rudin. Deep learning for case-based reasoning through prototypes: A neural network that explains its predictions. In *Proceedings of the AAAI Conference on Artificial Intelligence*, volume 32, 2018.
- [47] Bolei Zhou, Aditya Khosla, Agata Lapedriza, Aude Oliva, and Antonio Torralba. Learning deep features for discriminative localization. In *Proceedings of the IEEE Conference on Computer Vision and Pattern Recognition*, pages 2921–2929, 2016.
- [48] Ramprasaath R Selvaraju, Michael Cogswell, Abhishek Das, Ramakrishna Vedantam, Devi Parikh, and Dhruv Batra. Grad-CAM: Visual explanations from deep networks via gradient-based localization. In *Proceedings of the IEEE International Conference on Computer Vision*, pages 618–626, 2017.
- [49] German I Parisi, Jun Tani, Cornelius Weber, and Stefan Wermter. Lifelong learning of spatiotemporal representations with dual-memory recurrent self-organization. *Frontiers in Neuroinformatics*, page 78, 2018.
- [50] Michael Biehl, Barbara Hammer, and Thomas Villmann. Prototype-based models in machine learning. *Wiley Interdisciplinary Reviews: Cognitive Science*, 7(2):92–111, 2016.
- [51] Chen Liu, Guillaume Bellec, Bernhard Vogginger, David Kappel, Johannes Partzsch, Felix Neumärker, Sebastian Höppner, Wolfgang Maass, Steve B Furber, Robert Legenstein, and Christian G Mayr. Memory-efficient deep learning on a SpiNNaker 2 prototype. *Frontiers in Neuroscience*, 12:840, 2018.
- [52] Plamen P Angelov and Xiaowei Gu. *Empirical approach to machine learning*. Springer, 2019.
- [53] Plamen P Angelov and Xiaowei Gu. Deep rule-based classifier with human-level performance and characteristics. *Information Sciences*, 463:196–213, 2018.
- [54] Eduardo Soares and Plamen Angelov. Novelty detection and learning from extremely weak supervision. *arXiv preprint arXiv:1911.00616*, 2019.
- [55] Albert HR Ko, Robert Sabourin, Alceu de Souza Britto Jr, and Luiz Oliveira. Pairwise fusion matrix for combining classifiers. *Pattern Recognition*, 40(8):2198–2210, 2007.
- [56] Plamen Angelov. *Autonomous learning systems: From data streams to knowledge in real-time*. John Wiley & Sons, 2012.

- [57] Geoffrey J McLachlan. Mahalanobis distance. *Resonance*, 4(6):20–26, 1999.
- [58] Cornelius Weber and Stefan Wermter. A self-organizing map of sigma-pi units. *Neurocomputing*, 70(13-15):2552–2560, 2007.
- [59] Marvin Herchenbach, Dennis Müller, Stephan Scheele, and Ute Schmid. Explaining image classifications with near misses, near hits and prototypes: Supporting domain experts in understanding decision boundaries. In *Pattern Recognition and Artificial Intelligence: Third International Conference, ICPRAI 2022*, pages 419–430. Springer, 2022.
- [60] O. Russakovsky, J. Deng, H. Su, J. Krause, S. Satheesh, S. Ma, Z. Huang, A. Karpathy, A. Khosla, M. Bernstein, A. C. Berg, and F.-F. Li. ImageNet Large Scale Visual Recognition Challenge. *International Journal of Computer Vision*, 115:211–252, 2015.
- [61] A. Howard, M. Sandler, G. Chu, L.-C. Chen, B. Chen, M. Tan, W. Wang, Y. Zhu, R. Pang, V. Vasudevan, Q. V. Le, and H. Adam. Searching for MobileNetV3. In *Proceedings of the IEEE/CVF International Conference on Computer Vision*, pages 1314–1324, 2019.
- [62] Mark Sandler, Andrew Howard, Menglong Zhu, Andrey Zhmoginov, and Liang-Chieh Chen. MobileNetV2: Inverted residuals and linear bottlenecks. In *Proceedings of the IEEE Conference on Computer Vision and Pattern Recognition*, pages 4510–4520, 2018.
- [63] Mingxing Tan and Quoc Le. EfficientNet: Rethinking model scaling for convolutional neural networks. In *International Conference on Machine Learning*, pages 6105–6114. PMLR, 2019.
- [64] Kaiming He, Xiangyu Zhang, Shaoqing Ren, and Jian Sun. Deep residual learning for image recognition. In *Proceedings of the IEEE Conference on Computer Vision and Pattern Recognition*, pages 770–778, 2016.
- [65] Sylvestre-Alvise Rebuffi, Alexander Kolesnikov, Georg Sperl, and Christoph H Lampert. ICaRL: Incremental classifier and representation learning. In *Proceedings of the IEEE Conference on Computer Vision and Pattern Recognition*, pages 2001–2010, 2017.
- [66] Francisco M Castro, Manuel J Marín-Jiménez, Nicolás Guil, Cordelia Schmid, and Karteek Alahari. End-to-end incremental learning. In *Computer Vision: 15th European Conference, ECCV 2018*, pages 233–248, 2018.
- [67] Arthur Douillard, Matthieu Cord, Charles Ollion, Thomas Robert, and Eduardo Valle. PODNet: Pooled outputs distillation for small-tasks incremental learning. In *Computer Vision: 16th European Conference, ECCV 2020*, pages 86–102. Springer, 2020.
- [68] Yue Wu, Yinpeng Chen, Lijuan Wang, Yuancheng Ye, Zicheng Liu, Yandong Guo, and Yun Fu. Large scale incremental learning. In *Proceedings of the IEEE/CVF Conference on Computer Vision and Pattern Recognition*, pages 374–382, 2019.
- [69] Qi She, Fan Feng, Xinyue Hao, Qihan Yang, Chuanlin Lan, Vincenzo Lomonaco, Xuesong Shi, Zhengwei Wang, Yao Guo, Yimin Zhang, Fei Qiao, and Rosa H. M Chan. OpenLORIS-Object: A robotic vision dataset and benchmark for lifelong deep learning. In *2020 IEEE International Conference on Robotics and Automation (ICRA)*, pages 4767–4773. IEEE, 2020.
- [70] Bolei Zhou, Agata Lapedriza, Aditya Khosla, Aude Oliva, and Antonio Torralba. Places: A 10 million image database for scene recognition. *IEEE Transactions on Pattern Analysis and Machine Intelligence*, 40(6):1452–1464, 2017.
- [71] Tyler L Hayes, Nathan D Cahill, and Christopher Kanan. Memory efficient experience replay for streaming learning. In *2019 International Conference on Robotics and Automation (ICRA)*, pages 9769–9776. IEEE, 2019.
- [72] Saihui Hou, Xinyu Pan, Chen Change Loy, Zilei Wang, and Dahua Lin. Learning a unified classifier incrementally via rebalancing. In *Proceedings of the IEEE/CVF Conference on Computer Vision and Pattern Recognition*, pages 831–839, 2019.
- [73] Alexander Wong. NetScore: Towards universal metrics for large-scale performance analysis of deep neural networks for practical on-device edge usage. In *Image Analysis and Recognition: 16th International Conference, ICIAR 2019*, pages 15–26. Springer, 2019.
- [74] Wei Shiung Liew, Chu Kiong Loo, Vadym Gryshchuk, Cornelius Weber, and Stefan Wermter. Effect of pruning on catastrophic forgetting in growing dual memory networks. In *2019 International Joint Conference on Neural Networks (IJCNN)*, pages 1–8. IEEE, 2019.
- [75] Chayut Wiwatcharakoses and Daniel Berrar. SOINN+, a self-organizing incremental neural network for unsupervised learning from noisy data streams. *Expert Systems with Applications*, 143:113069, 2020.
- [76] Aleksej Logacjov, Matthias Kerzel, and Stefan Wermter. Learning then, learning now, and every second in between: lifelong learning with a simulated humanoid robot. *Frontiers in Neurobotics*, 15:669534, 2021.

- [77] Alan H Gee, Diego Garcia-Olano, Joydeep Ghosh, and David Paydarfar. Explaining deep classification of time-series data with learned prototypes. In *CEUR Workshop Proceedings*, volume 2429, page 15. NIH Public Access, 2019.
- [78] Eoin M Kenny and Mark T Keane. Explaining deep learning using examples: Optimal feature weighting methods for twin systems using post-hoc, explanation-by-example in xai. *Knowledge-Based Systems*, 233:107530, 2021.
- [79] Laurens Van der Maaten and Geoffrey Hinton. Visualizing data using t-SNE. *Journal of Machine Learning Research*, 9(11):2579–2605, 2008.
- [80] Sheng-Jun Wang and Changsong Zhou. Hierarchical modular structure enhances the robustness of self-organized criticality in neural networks. *New Journal of Physics*, 14(2):023005, 2012.
- [81] Atiq Ur Rehman and Samir Brahim Belhaouari. Divide well to merge better: A novel clustering algorithm. *Pattern Recognition*, 122:108305, 2022.

Supplementary Materials

.1 Visualization of the Places-365 topology

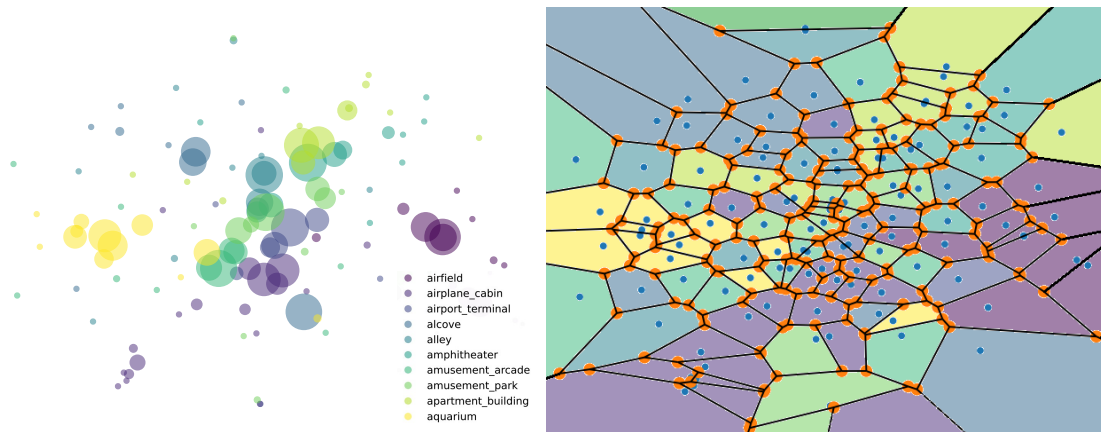


Figure 7: Visualizing the topology of learned prototypes acquired from the Places-365 dataset, for the first 10 classes. On the left is a 2-dimensional representation of the identified prototypes generated using t-SNE. Each circle represents one prototype and the radius of each circle denotes the support for that prototype. On the right is the generated Voronoi tessellation.

Figure 7 visualizes the topology of the prototypes encoded using ExLL-F. In the left sub-figure, the high-dimensional centroids are transformed into 2-dimensional scatter plots using t-distributed stochastic neighbor embedding (t-SNE) [79]. Each circle denotes one prototype and the radius of the circle indicates the support or size of the prototype’s data cloud. There are multiple instances where neighbouring prototypes displayed overlapping areas of influences. The presence of overlap suggests that some prototypes are highly similar to each other even after self-organization. It is possible to reduce redundancies by merging the overlapping prototypes, for example, by using hierarchical clustering [80] or divide-and-merge [81]. In the right sub-figure, the same 2-dimensional prototype topology is represented using a Voronoi tessellation graph. The merged prototypes, for instance, may be visualized by removing the edges between neighbouring partitions with the same colour (i.e., same class labels).

.2 Visualization of the F-SIOL-310 topology

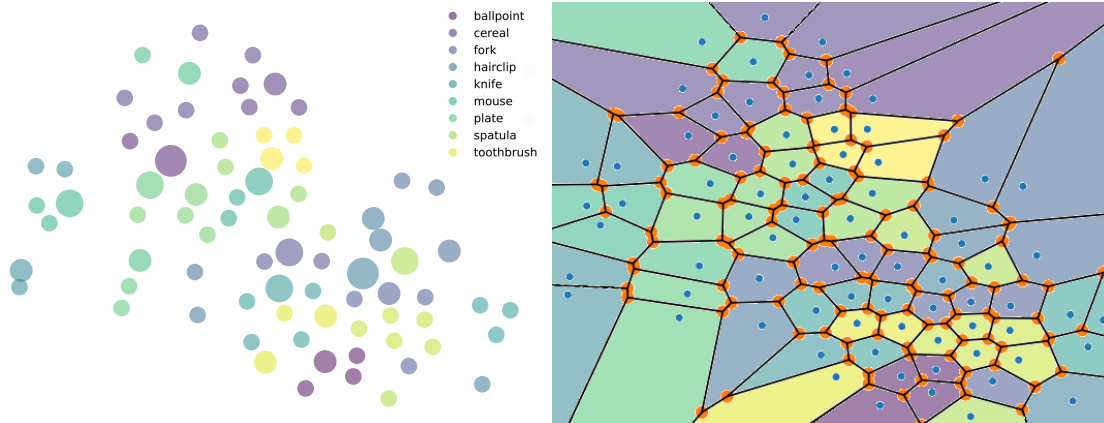


Figure 8: Visualizing the topology of learned prototypes acquired from the F-SIOL-310 dataset. On the left is a 2-dimensional representation of the identified prototypes generated using t-SNE. Each circle represents one prototype and the radius of each circle denotes the support for that prototype. On the right is the generated Voronoi tessellation.

Figure 8 visualizes the topology of the prototypes encoded using ExLL-F. In the left sub-figure, the high-dimensional centroids are transformed into 2-dimensional scatter plots using t-SNE. Each circle denotes one prototype and the radius of the circle indicates the support or size of the prototype’s data cloud. The prototypes encoding the F-SIOL-310 dataset form a highly-separable topology with clear delineation between prototypes. This is considerably different compared to the Places topology in Figure 7. The difference may be due to the visually distinctive objects in the F-SIOL-310 dataset while the Places dataset has significantly more variety of images within-class causing the overlap. Similarly in the right sub-figure, the Voronoi tessellation graph for F-SIOL-310 displayed a distribution of evenly spaced cells highlighting the prototype separability.